The Physics of Chromospheric Plasmas
ASP Conference Series, Vol. 368, 2007
Petr Heinzel, Ivan Dorotovič and Robert J. Rutten, eds.

Observing the Solar Chromosphere

Robert J. Rutten
Sterrekundig Instituut, Utrecht University, The Netherlands
Institutt for Teoretisk Astrofysikk, University of Oslo, Norway

Abstract. This review is split into two parts: one on chromospheric line formation in answer to the frequent question "where is my line formed", and one presenting state-of-the-art imagery of the chromosphere. In the first part I specifically treat the formation of the Na D lines, Ca II H&K, and Hα. In the second I show DOT, IBIS, VAULT, and TRACE images as evidence that the chromosphere consists of fibrils of intrinsically different types. The straight-up ones are hottest. The slanted ones are filled by shocks and likely possess thin transition sheaths to coronal plasma. The ones hovering horizontally over "clapotispheric" cell interiors outline magnetic canopies and are buffeted by shocks, most violently in the quietest regions.

In the absence of integral-field ultraviolet spectrometry, Hα remains the principal chromosphere diagnostic. The required fast-cadence profile-sampling imaging is an important quest for new telescope technology.

1. Introduction

An excellent review of observational chromospheric issues and research is given by Philip G. Judge in the 2005 NSO/Sacramento Peak workshop proceedings (Judge 2007; `http://download.hao.ucar.edu/pub/judge/judge_ws23.pdf`). His major conclusion is that while chromospheric magnetism smoothes out with height, its thermal fine structuring remains tremendous. Here, I tread less wide by concentrating on diagnostics of this fine structure, in particular those in the visible. Long-duration observing with Hinode's SOT and higher-resolution observing exploiting adaptive optics at existing telescopes (DST, VTT, SST) and hopefully at upcoming telescopes (GREGOR, NST, EST, ATST) employing Ca II H&K, the Ca II infrared lines, and above all the H I Balmer lines are likely to provide new high-resolution vistas and understanding of the chromosphere the coming years while, unfortunately, ultraviolet spectrometry lags behind. I split the discussion into a didactic part on chromospheric line formation and a morphological part on chromospheric scenes, concluded by a list of speculations and a brief discussion of research approaches.

2. Chromospheric Line Formation

As author of lecture notes on radiative transfer (Rutten 2003a) I am often asked how high some line is formed. In this section I follow the inspiring "Fads and Fallacies" example of Athay (1976) to illustrate that the question is only answerable for numerical models or simulations, not for observations.

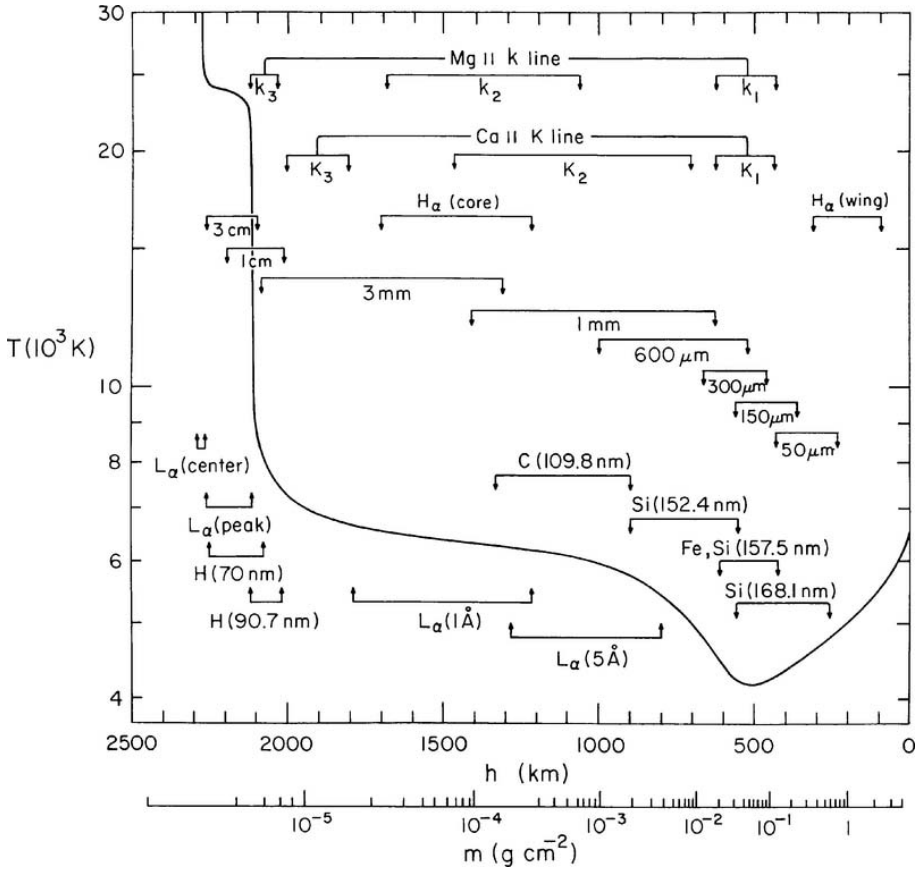

Figure 1. Classic VAL3C height-of-formation graph from Vernazza et al. (1981). The bars span 90% of the area under the intensity contribution functions $\mathrm{d}I/\mathrm{d}h$ plotted for many wavelengths in Fig. 36 of the same paper.

The answer evolved over the years from "weighting functions" (e.g., Pecker 1951, Unsöld 1955) through "line-depression contribution functions" (e.g., Edmonds 1967; Gurtovenko & Ratnikova 1974; Magain 1986; Kucera et al. 1998) to "response functions" (e.g., Mein 1971; Beckers & Milkey 1975; Caccin et al. 1977) which became the backbone of least-square-fit inversions with the SIR code of Ruiz-Cobo et al. (1990, 1992) and its companions (see del Toro Iniesta 2003; Cabrera Solana et al. 2005). I discuss the answer first in the context of solar-atmosphere model evolution, and then for some specific lines.

2.1. HOLMUL, SIR, VAL3C, RADYN, CO^{5}BOLD chromospheres

For decades already, stellar abundance determiners prefer the HOLMUL model of Holweger & Müller (1974) in the classical Unsöld "fine analysis" recipe of computing stellar line formation as plane-parallel hydrostatic LTE with best-fit microturbulence and van der Waals damping enhancement but no other pa-

rameters (cf. Rutten 1998, 2002). The HOLMUL temperature stratification is essentially Holweger's (1967) empirical fit to many observed optical lines, from iron in particular, assuming LTE excitation and ionization. Actual iron-line NLTE departures (mainly smaller opacity due to overionization for weaker Fe I lines, source function deficit due to scattering for the strongest Fe I lines, and source function excess for pumped subordinate Fe II lines) happen to largely cancel in this procedure over much of the optical spectrum (Rutten & Kostik 1982), so that the model performs very well in reproducing any line similar to the ones from which it was made, under the same assumptions. It does not possess a chromospheric temperature rise because iron lines exhibit no self-reversals.

The Holweger technique of empirically establishing a temperature-height stratification by fitting excitation temperatures and optical depth scales to observed lines assuming LTE is automated in the SIR code for Stokes evaluation. It effectively constructs such Holweger models per pixel. They won't have chromospheres either, except when inverting the Mg I 12-micron lines which do show conspicuous reversals – but then wrongly because their emission peaks are actually photospheric NLTE ones (Carlsson et al. 1992). Another key inversion assumption is that solar stratifications vary smoothly with height, as cubic splines through only a few sampling nodes. This is a dangerous assumption when large fluctuations occur, such as the shocks making up umbral flashes (cf. Socas-Navarro et al. 2001).

The VAL3C model of Vernazza et al. (1981) differs from the Holweger approach in primarily fitting continua rather than lines but extends much higher by including the full ultraviolet, necessitating detailed NLTE evaluation of many bound-free edges and PRD evaluation of Ly-α. This model is elevated to stellar status ("the star VAL3C") in my lecture notes because it represents a complete self-consistent numerical simulation of the radiation from a time-invariant plane-parallel star which strictly obeys all standard equations in my course (plus some more, because the latter do not yet treat PRD whereas the Avrett-Loeser PANDORA code does) while resembling the sun (at least spectrally) in having a chromosphere and some sort of transition region to a coronal regime. The magnificent VAL3 paper adds a superb collection of informative graphs diagnosing for many frequencies how this star radiates, where its radiation originates, and breaking down its radiative energy budget. The FALC model of Fontenla et al. (1993) and more recent ones by e.g., Fontenla et al. (2006) represent updates of the approach with a similar code. Figure 1, perhaps the best-known graph of solar physics, shows heights of formation for many VAL3C diagnostics. In the star VAL3C these are rigorously correct. Are they in the sun?

For example, the chromospheric dynamics analysis of Bloomfield et al. (2004) relied on the VAL3C height difference between Hα and Ca II K core formation, the latter higher than the former, to estimate upward propagation speeds and so assign particular MHD wave modes and appropriate mode conversions to a few observed oscillation wave trains through wavelet analysis of network bright points in filtergrams. The approach is interesting but the reliance on VAL3C formation heights, with Ca II K higher up than Hα, is naïve even if purely radial structures were indeed observed in both lines (see Fig. 6). I feel that numerical wave simulation comparing detailed Hα and Ca II K line synthesis using a detailed model of such a structure is a sine-qua-non step in such mode identification.

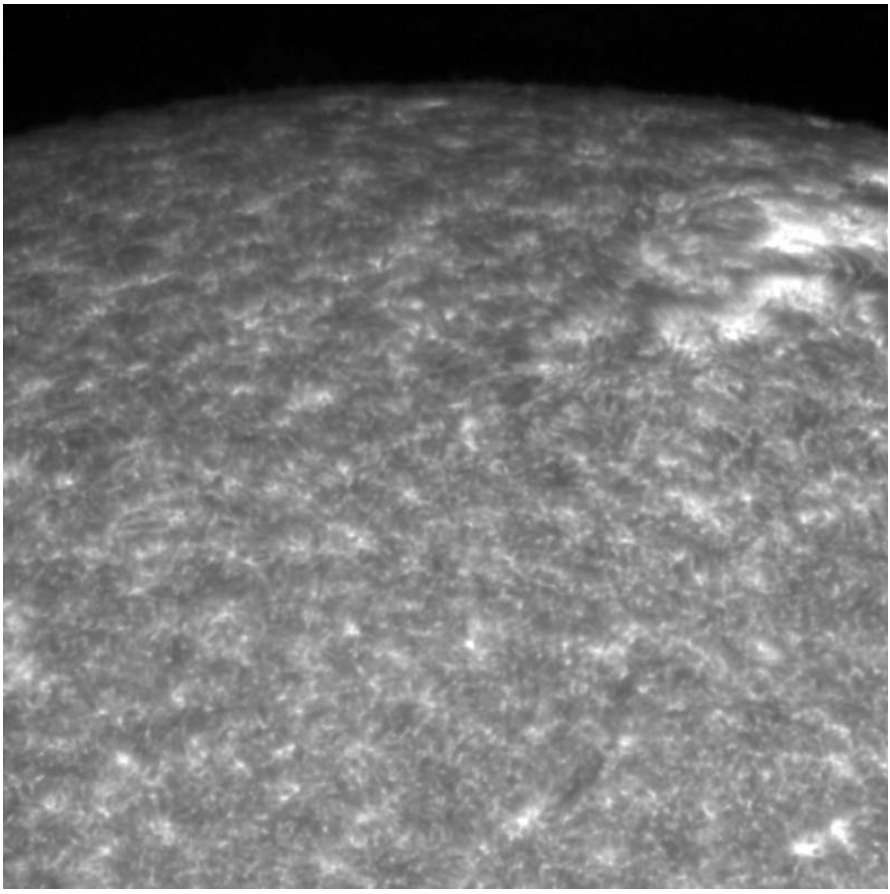

Figure 2. Another classic: part of a Ca II K_{2V} spectroheliogram taken by B. Gillespie at Kitt Peak thirty years ago. Other cutouts appeared on the cover of Lites (1985), in Zirin (1988), in Rutten & Uitenbroek (1991b), as frontispiece to Solar Phys. 134, and elsewhere. Outside active areas this image displays the solar clapotisphere rather than the solar chromosphere. Courtesy K. P. Reardon.

Detailed wave simulation was undertaken for the much easier case of purely acoustic waves sampled by the 170 nm and 160 nm bandpasses of TRACE by Fossum & Carlsson (2005a, 2005b, 2006) using the RADYN code of Carlsson & Stein (e.g., 1992, 1997). These ultraviolet continua suffer considerable NLTE Si I bound-free scattering, as is obvious in the pertinent Fig. 36 *B-J-S* panels of VAL3, but at least this scattering obeys complete frequency redistribution over the ionization edge. Fossum & Carlsson included it in evaluating brightness response to acoustic-wave perturbations. They first explained the puzzling high-frequency phase-difference behavior observed by De Wijn et al. (2005) as due to doubly-peaked 170 nm response, and they then evaluated the amount of observed high-frequency power as not enough to heat the chromosphere.

The latter result is questioned on p. 93 ff of this book by Wedemeyer-Böhm et al. (2007) who compute synthetic 160 nm images from CO^{5}BOLD simulations in LTE, without and with magnetic fields, to claim that the RADYN code by being only one-dimensional severely underestimates acoustic heating through the small-scale high-frequency acoustic interference patterns found in the 3D CO^{5}BOLD atmosphere at about $h = 500$ km. I have called such a quiet-sun regime where wave interference acts as the dominant structuring agent, above the overshooting convection but still below a magnetic canopy, a "*clapotisphere*" (Rutten 1995), inspired by Carlsson (1994) and the reference in Rutten & Uitenbroek (1991a) to Dowd (1981). While the grey CO^{5}BOLD star does not (yet) possess a fibrilar magnetism-dominated chromosphere as the solar one displayed in Section 3 below, it surely has a violent clapotisphere, even in excess of RADYN's.

Does the sun possess a clapotisphere? Yes, see the much-published spectroheliogram in Fig. 2. Selecting the special Ca II K_{2V} passband emphasizes acoustic shocks as "cell grains" in internetwork areas (Rutten & Uitenbroek 1991a). They are brightest in H_{2V} and K_{2V} through intricate vertical shock interference explained beautifully in Figs. 4–7 of Carlsson & Stein (1997), but remain visible through wider passbands (Fig. 10 of Krijger et al. 2001).

Which of the VAL3C, RADYN, and CO^{5}BOLD chromospheres resembles the solar one the best? In the VAL3C star the resonance lines of Mg II and Ca II are the major chromospheric cooling agents and require NLTE–PRD synthesis. RADYN neglects h&k and assumes CRD for H&K (perhaps mutually corrective since line cooling is too large in CRD due to deeper photon escape through the wings) but adds the virtue of computing time-dependent ionization. CO^{5}BOLD has the virtue of being 3D but unrealistically assumes grey LTE radiative transfer at all heights, ignoring actual strong-line cooling, lack of surface cooling through scattering, and fast-versus-slow asymmetry between ionization and recombination in and behind shocks (Carlsson & Stein 2002). It may so overestimate the occurrence of fine structure (Leenaarts & Wedemeyer-Böhm 2006).

The verdict is not in. Let us regard VAL3C, RADYN, and CO^{5}BOLD as interesting stars with sun-like photospheres but chromospheres that exist only computationally. VAL3C assumes that temperature fluctuations around the mean are small enough to be meaningfully averageable. RADYN's shocks deny such averaging but do not generate ultraviolet line emission. CO^{5}BOLD has more acoustic heating but its grey-LTE-instantaneous radiative cooling is very non-solar.

My feeling remains that the actual solar chromosphere is hot where the field points up or fans out from network and plage, that the internetwork is cool below the canopy except within shocks, that the latter clapotispheric domain represents a wide radial gap in H&K emissivity and Hα opacity, and that chromospheric internetwork radiation in Hα, the Ca II infrared lines and all ultraviolet lines including Ly-α comes from canopy-constituting mottles/fibrils/spicules and their sheath-like boundary layers. I gave some evidence in Rutten (2007) and give some more in Section 3 below.

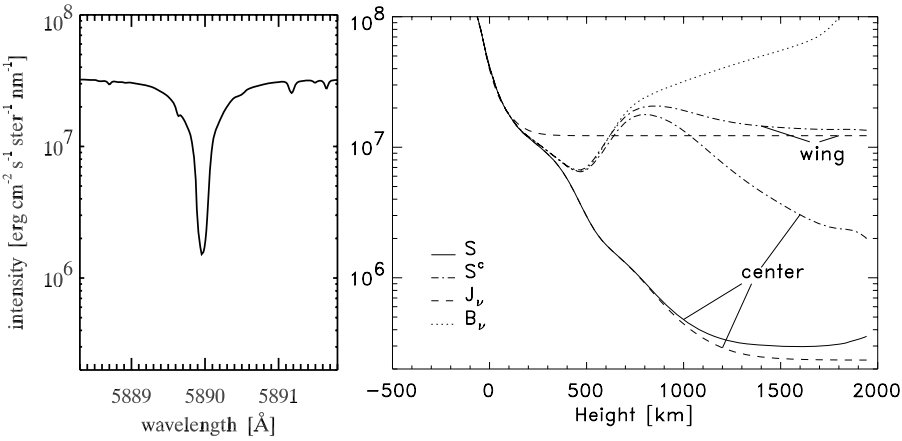

Figure 3. Formation of the Na D$_2$ line. Lefthand panel: disk-center line profile from the Kitt Peak FTS atlas (Neckel 1999) plotted on the same logarithmic scale as the S,B,J line-formation graph at right from Uitenbroek & Bruls (1992). The Na D$_2$ line is deep because its source function sinks deep, far below the temperature minimum. The model shown by the dotted B_ν curve is actually FALC of Fontenla et al. (1993), whose photosphere copied the VAL3C update of Maltby et al. (1986) which effectively brought the significantly-cooler-than-HOLMUL upper photosphere of VAL3C back to HOLMUL (and to near-radiative-equilibrium and near-LTE iron ionization) through the inclusion of a great many NLTE-scattered ultraviolet line haze lines in PANDORA (cf. Avrett 1985; Rutten 1990), but Uitenbroek & Bruls maintained the name VALC. At line center, the total source function equals the line source function which closely mimics a two-level atom dominated by scattering with complete redistribution. You may refresh your grasp of line formation by estimating ε and working out why the background continuum source function differs between line center and wing (hint: why does $S^c_{\rm wing} \Rightarrow J_{\rm wing}$ at right?).

2.2. Na I D in VAL3C

Figure 3 diagnoses Na I D formation in VAL3C didactically. The Eddington-Barbier relation $I_\nu \approx S_\nu(\tau_\nu = 1)$ suggests, through simply drawing a horizontal line from line center at left to the solid curve at right, that Na D$_2$ line center originates at $h \approx 600$ km. It is more like $h \approx 800$ km in Bruls et al. (1992) but in any case $\tau_\nu = 1$ lies in the VAL3C chromosphere, i.e. above the temperature minimum. Contribution functions to the emergent intensity or to the line depression will put the core formation there too. However, the intensity is obviously dominated by scattered photons originating much deeper: the line-center source function doesn't appreciate that VAL3C possesses a chromosphere. The Na D lines are often called chromospheric but their VAL3C brightness response is photospheric. Only when studying Na D Dopplershift may one call these lines chromospheric (assuming a VAL3C-like chromosphere) because the Dopplershift is encoded at the last photon scattering towards the observer. Thus, the "magnetoacoustic portals" analysis of Jefferies et al. (2006) comparing Na I to K I

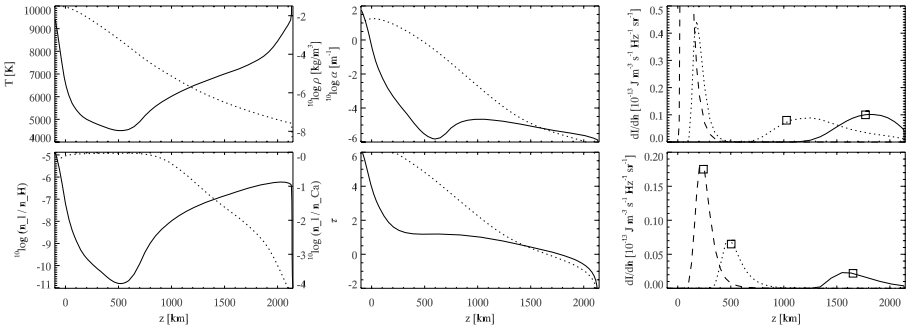

Figure 4. Didactic explanation of the difference between Hα and Ca II H formation assuming LTE, taken from Leenaarts et al. (2006). *Top left*: FALC temperature (lefthand scale, solid) and density (righthand scale, dotted). *Bottom left*: population fraction of the lower level relative to the total species density, respectively for Hα (lefthand scale, solid) and for Ca II H (righthand scale, dotted). *Top center*: line-center extinction coefficient for Hα (solid) and Ca II H (dotted). *Bottom center*: line-center optical depth for Hα (solid) and Ca II H (dotted). *Top right*: Hα intensity contribution functions for $\Delta\lambda = 0$ (solid), -0.038 (dotted), and -0.084 nm (dashed) from line center. Squares mark $\tau = 1$ locations. *Bottom right*: the same for Ca II H, at $\Delta\lambda = 0$ (solid), -0.024 (dotted), and -0.116 nm (dashed) from line center.

Dopplershifts rightfully claims measurement at the bottom of the chromosphere, whatever that may be.

Let me ask you some examination questions. Where is $\tau_\nu = 1$ for the weak blend at $\lambda = 5888.6$ Å in the lefthand panel of Fig. 3? Should you compute an intensity or a line depression contribution function for it? Is Milne-Eddington or Schuster-Schwarzschild the better approximation for inversion? Well, drawing the Eddington-Barbier connecting line locates $\tau_\nu = 1$ at about $h = 100$ km, right? Fitting a Milne-Eddington line-depression contribution would be your first bet in modeling such a weak line, right? Wrong! And not a little either. The line is due to water vapor in our own atmosphere, a million times higher up than your estimate, and Schuster-Schwarzschild is the better description.

2.3. Ca II H and Hα in FALC

Figure 4 compares Hα formation to Ca II H formation in FALC assuming LTE which holds reasonably well in the wings of these lines. The difference is enormous!

Ca II H originates from the ground state of the dominant ionization stage, containing virtually all calcium particles out to $h \approx 800$ km where ionization (taking only 11.9 eV) to Ca III sets in (row 2 panel 1), and so has smooth sampling throughout the lower atmosphere with near-constant inward τ_ν build-up, resulting in nice single-peaked intensity contribution functions which smoothly shift outward closer to line center. The extended Ca II H&K wings present an ideal probe to step smoothly through the lower atmosphere, also furnishing blends for Doppler and Zeeman sampling as diagnostics ripe for SIR inversions.

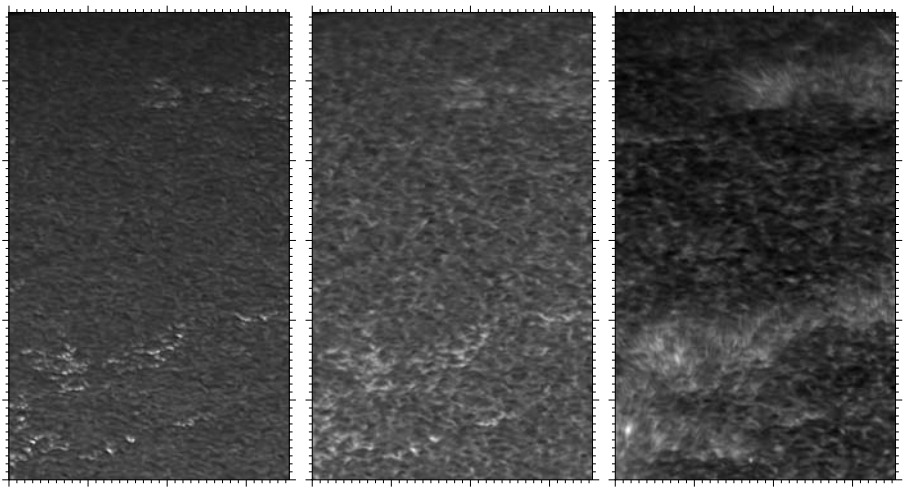

Figure 5. Three partial near-limb images taken with the DOT on June 18, 2003. Ticks at arcsec intervals. *Left*: G band. *Center*: Ca II H wing. *Right*: Ca II H line center. From Rutten (2007).

In contrast, Hα originates from the extremely temperature-sensitive $n=2$ level at 10.2 eV, and so has a pronounced formation gap around the temperature minimum, no τ_ν buildup there, and double-peaked contribution functions as already shown by Schoolman (1972): in Hα one either observes the deep photosphere or the overlying chromosphere.

3. Chromospheric Scenes

In this section I insert images from the DOT[1], IBIS, and VAULT to demonstrate that the chromosphere is intrinsically fibrilar (with the term "fibrils" encompassing quiet-sun "mottles" and off-limb "spicules"). This message is far from new (e.g., Zirin 1988) but the state-of-the-art images in Figs. 5–12 deliver it beyond any wishful 1D thinking.

3.1. Ca II H&K and Hα chromosphere

Figure 5 shows at left the onset of reversed granulation and "faculae", the latter as short bright stalks where our slanted G-band view penetrates through relatively empty network fluxtubes into hot granule tops as sketched in Fig. 7 of Rutten (1999a) and more recently in Fig. 4 of Keller et al. (2004). The center panel shows a similar scene sampled slightly higher up. The third panel shows a dark wing-contributed background of reversed granulation with some shock interference wherever there is insignificant magnetic-feature emission in

[1] All available at `ftp://dotdb.phys.uu.nl` with a convenient search interface at `http://dotdb.phys.uu.nl/DOT`.

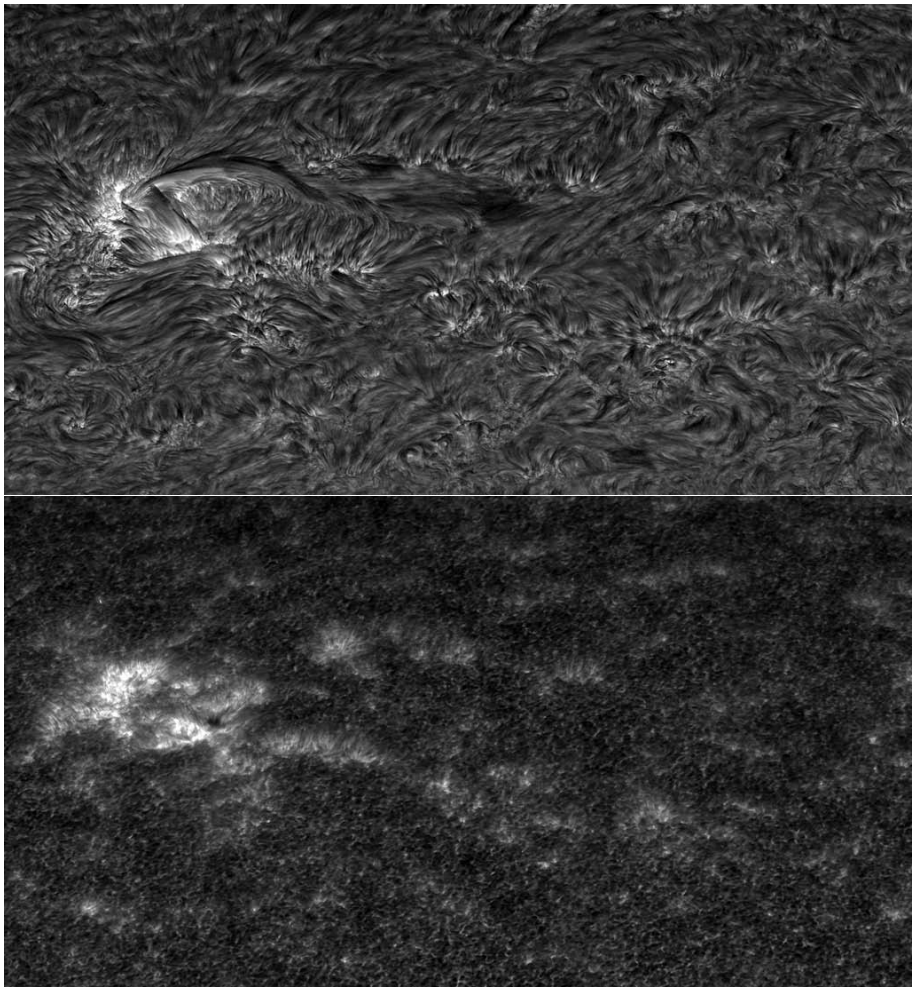

Figure 6. Simultaneous image mosaics taken with the DOT on October 4, 2005, respectively in Hα and Ca II H. The field of view is close to the limb (off the top) and measures about 265×143 arcsec^2.

the Ca II H core. The active network shows up through clusters of long, thin, bright features added by the line core. They start at photospheric faculae, are sharply delineated from the dark background in their foreground, appear to be optically thin, and stand rather upright causing overall hedge-row appearance. They make up the bright patches in the narrower-band image in Fig. 2. The movie from which this frame is taken shows that they are very dynamic. I called them "straws" in Rutten (2007). They are only seen at high resolution, meaning angular rather than spectral resolution. In fact, it is better to use a fairly wide passband to catch the emission peak whatever its Dopplershift. Adding inner-

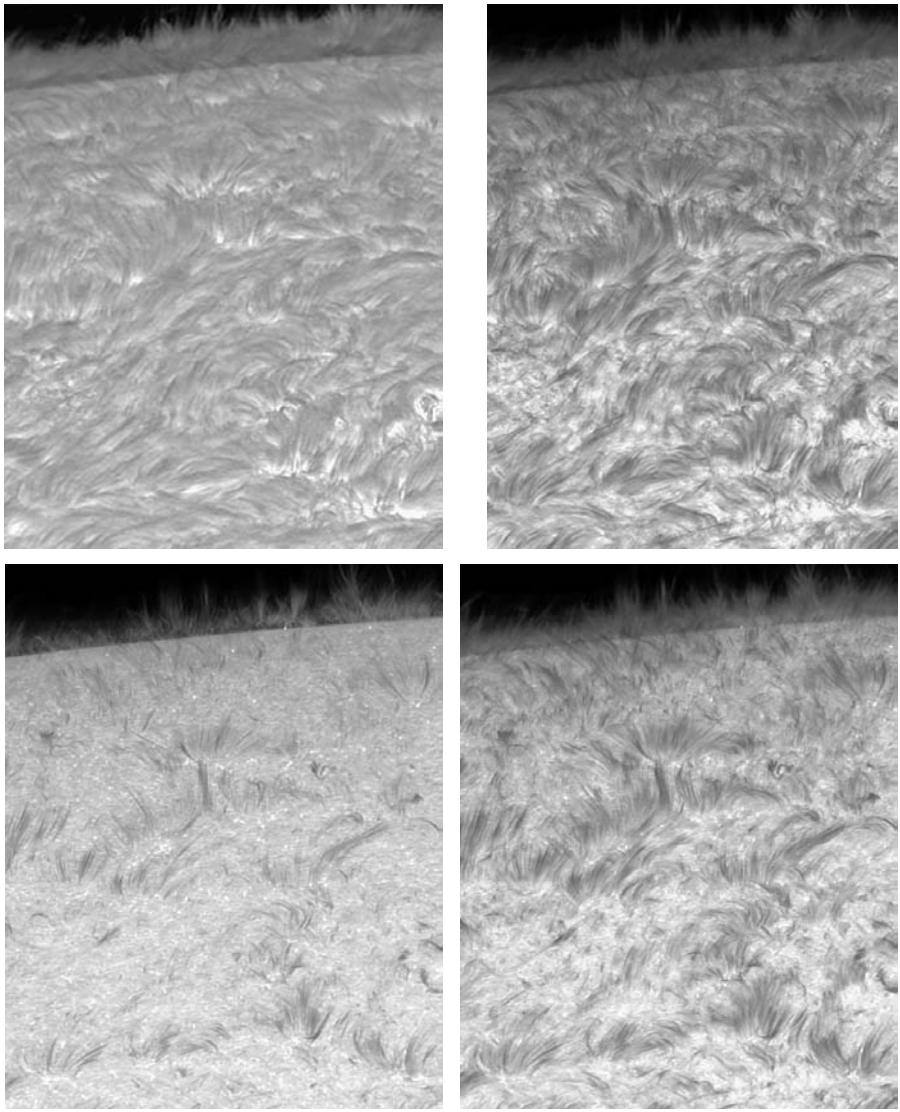

Figure 7. Profile-sampled Hα fine structure near and at the limb, taken with the DOT on October 4, 2005. Clockwise: line center, $\Delta\lambda = -400$, -600, -800 mÅ, not simultaneous but all four taken within one minute. Field of view about 70×85 arcsec^2.

wing reversed-granulation background poses no problem because this is quite dark.

Figure 6 is a similar but higher-up near-limb scene comparison, between Ca II H and Hα. The Ca II H image again shows much dark photospheric background with bright network hedges and straw crowding in the small active region.

In contrast, Hα is chromospheric nearly everywhere, with fibrils covering internetwork cells in a fibrilar canopy. The comparison immediately repudiates the notion that Ca II H is formed higher than Hα. The lower panel shows only the onset of the chromosphere, the upper one the full monty.

Figure 7 samples the limb part of this field while stepping the DOT Hα filter through the line. The line-center image again shows a mass of cell-spanning fibrils as a flattened carpet, with upright ones jutting out from network. I doubt that the double limb is caused by parasitic light (continuum leak outside the Hα passband): the lower limb is bumpy (zoom in with a viewer) and seems to mark the top of the carpet, the upper limb the end of hedge-row visibility. We have no DOT movie yet of off-limb spicules, but many are bound to bounce up and down with 3–5 min periodicity – perhaps fading on their return to convey the classical notion that spicules send up much more mass then comes down. Their upper ends correspond to the tops of "dynamic fibrils" as those observed on-disk with the SST on the same glorious day and analyzed in detail in the beautiful paper of De Pontieu et al. (2007).

The off-limb line-center fibrils constitute the authentic "chromosphere" because this name comes from their Hα emission during totality. Since there is no intrinsic difference between off-limb fibrils and on-disk fibrils (they don't care about our location in their sky), the proper definition of "chromosphere" is simply the mass of fibrils observed in Hα.

The other panels show the same scene progressively further out into the blue Hα wing. At decreasing line opacity one sees more and more photospheric background (not even granularly reversed) between the hedge rows. In the outer wing only rather upright fibrils in network hedge rows remain, appearing as dark to very dark strands against the deep-photosphere background and across the continuum limb. J. Leenaarts has pointed out that the latter is much brighter than the high-photosphere background seen in Ca II H, making straws dark in Hα while bright in Ca II H&K. In addition, Doppler shifts may darken them further by shifting the line core into the passband. A. G. de Wijn has suggested that Hα outer-wing darkness may also result from excessive Hα line width due to high temperature.

Let us now move to disk center. Figure 8 shows an area containing active network in Ca II H center and H$\alpha - 0.3$ Å. The slender bright stalks jutting out from the network, seen in Ca II H but only at high angular resolution, are the on-disk representation of the near-limb straws. Blinking shows that they usually coincide with the lower ends of bright Hα fibrils. Many of the latter span much further out across the internetwork. In Ca II H the latter is dark with reversed granulation and therefore photospheric or clapotispheric but not chromospheric. Hα shows fibrils over much longer lengths than Ca II H, implying large heights since Ca II H straws are preferentially upright. However, in the upper-right corner of this cut-out field the Hα wing shows short and grainy fine structure in a very quiet area, possibly as chromospheric transparency into either the top of the clapotisphere or the deep photosphere.

Figure 9 display an extremely quiet region. The Hα line-center scene shows much less large-scale organization than for more active areas. Most fibrils are short and strongly curved. In many places the Hα chromosphere appears optically thin. The two summed-wing images (second row) confirm this: the $\Delta\lambda = -700$ mÅ one shows only parts of fibrils close to the scarce and sparse

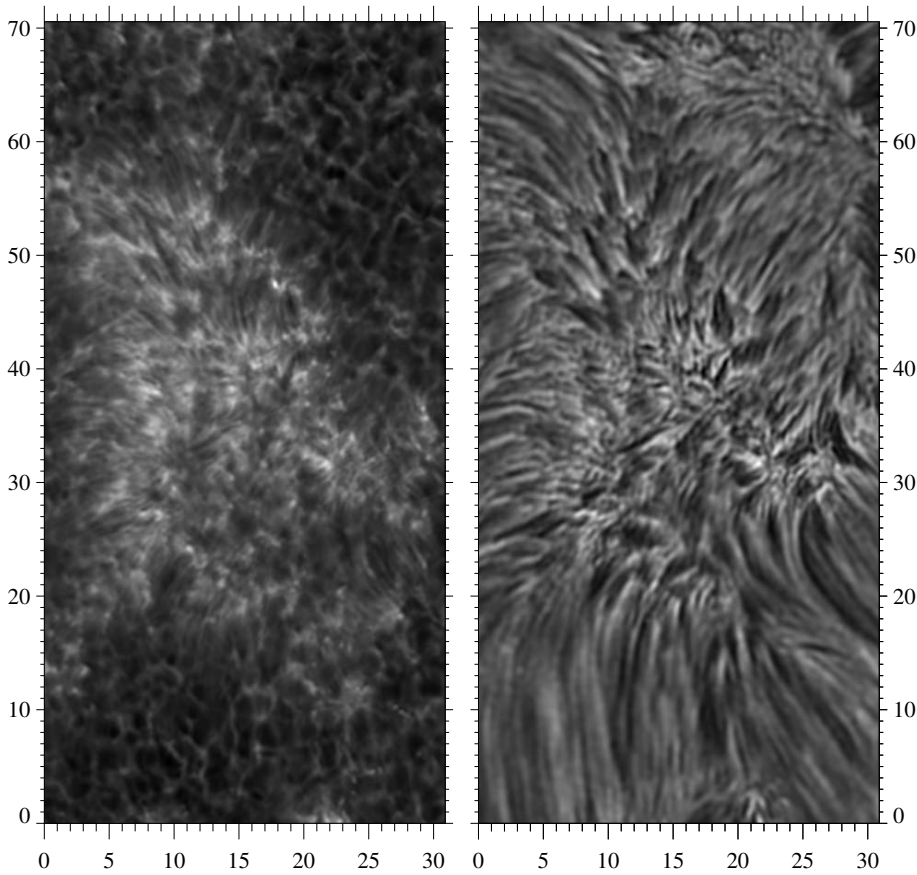

Figure 8. Two partial on-disk images taken with the DOT on April 24, 2006. Scales in arcsec. *Left*: Ca II H. *Right*: Hα − 350 mÅ. Courtesy P. Sütterlin.

network. The $\Delta\lambda = -350$ mÅ Dopplergram (third row) shows as much confusion as the line-center image. These samples come from a 71-minute multi-wavelength DOT sequence with half-minute cadence (one minute for the Hα wing wavelengths between which the filter switched alternatively). Movies from these data show that this cadence is much too slow. The quietest areas on the solar surface are least stable in Hα.

Figure 10 indicates why. The occurrence of an "acoustic event" is diagnosed by the sudden appearance of a bright repetitive grain in Ca II H. It follows on the squeezing away of a small granular shard by converging large granules, just as the "collapsars" of Skartlien et al. (2000). The Hα line-center brightness does not react markedly but there is large response in both Doppler samplings, most clearly seen in the time slices: sudden onset of oscillation wave trains with upward increasing amplitude. Their spatial extent, 4 arcsec, is much wider than the piston or the Ca II H grain, suggesting that an extended piece of elastic canopy responds to the shock buffeting from below. This area is also quiet,

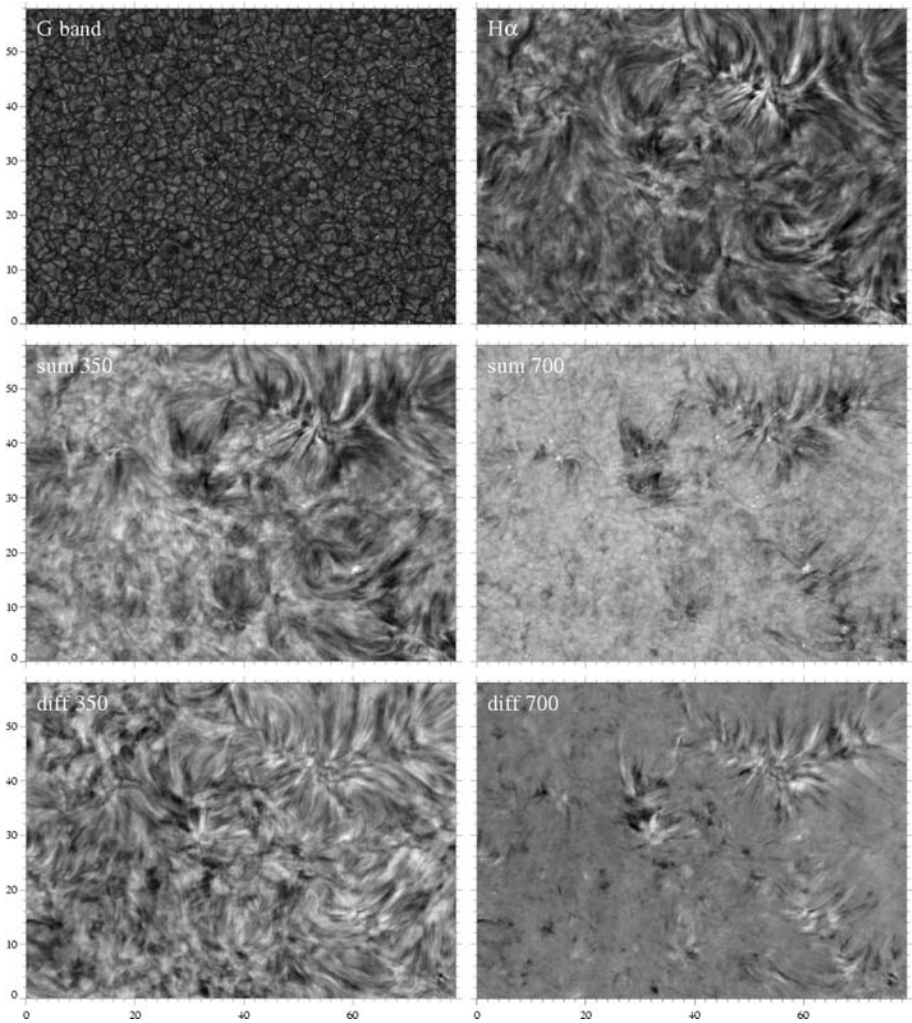

Figure 9. Very quiet disk-center scene taken with the DOT on October 19, 2005. *Upper row*: G band and Hα center. *Middle row*: sums of Hα wing brightness at $\Delta\lambda = \pm 350$ and ± 700 mÅ. *Bottom row*: differences of these wing pairs (Dopplergrams, blueshift dark). Scales in arcsec. Courtesy P. Sütterlin.

indeed without evident fibrilar structuring. The time slices indicate that most of the small-scale Hα brightness patterning is of oscillatory nature.

3.2. Ca II IR chromosphere

Figure 11 shows the chromosphere as it appears in Ca II 8542 Å. The bottom panels resemble Hα rather than Ca II H in Fig. 8. At various occasions I have wondered how this subordinate calcium line can be more chromospheric than its

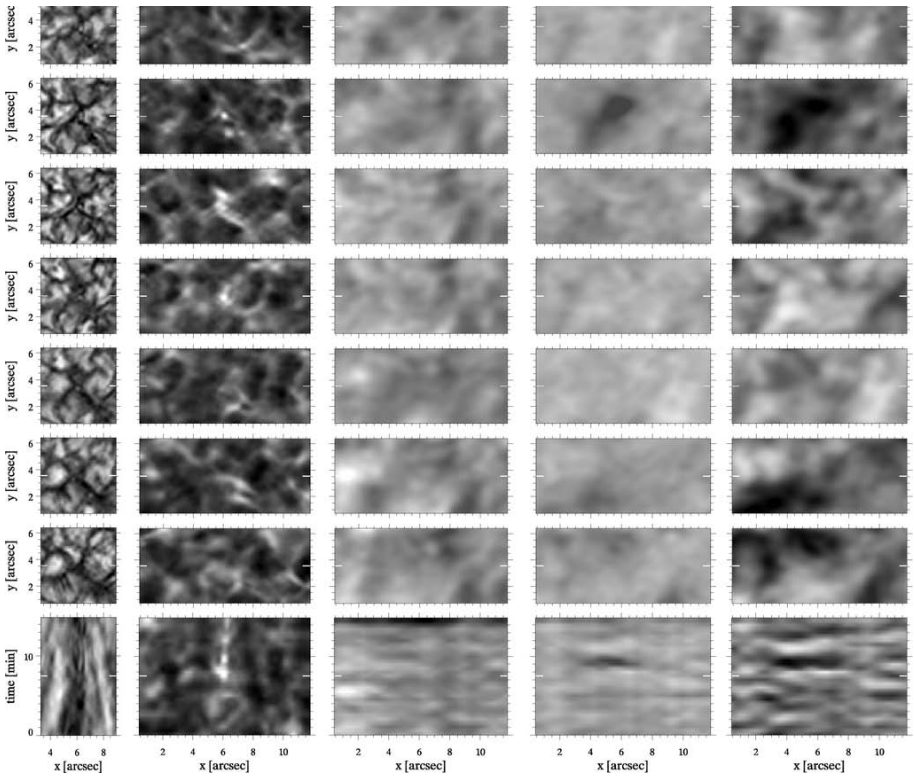

Figure 10. Hα response to an acoustic event, from DOT images taken on October 14, 2005. The first seven rows are small image cutouts, respectively G band, Ca II H center, Hα center, and Hα Dopplergrams from $\Delta\lambda = \pm 700$ mÅ wing pairs and from $\Delta\lambda = \pm 350$ mÅ wing pairs. Bright implies blueshift in the latter two. The cutouts are wider for Ca II H and Hα in order to show more context in the $x-t$ time slices in the bottom panels. The latter show the brightness evolution along the horizontal cut through the center of the subfield defined by the white markers in each image cutout. The time step between consecutive image rows is one minute, with time increasing from bottom to top in correspondence with the time direction in the slices. The image sequence is centered in time (fourth row, white markers in the slices) on the first appearance of a bright Ca II H grain. Courtesy B. van Veelen.

resonant H&K siblings with larger opacity. The habitual answer of G. Cauzzi, H. Uitenbroek and M. Carlsson is that the sizable excitation energy of its lower level gives larger temperature sensitivity and that the steep flanks of its narrower line profile give larger Doppler sensitivity, and that these combine to pick up fibril signatures that are less evident in H&K filtergrams. Reardon et al. illustrate the point further on p. 151 ff in these proceedings.

In large active regions one can often trace dark fibrils in Ca II H if one knows where they are from Hα, but they appear much clearer in Ca II 8542, with enhanced small-scale contrast in the inner-wing panel of Fig. 11, presumably

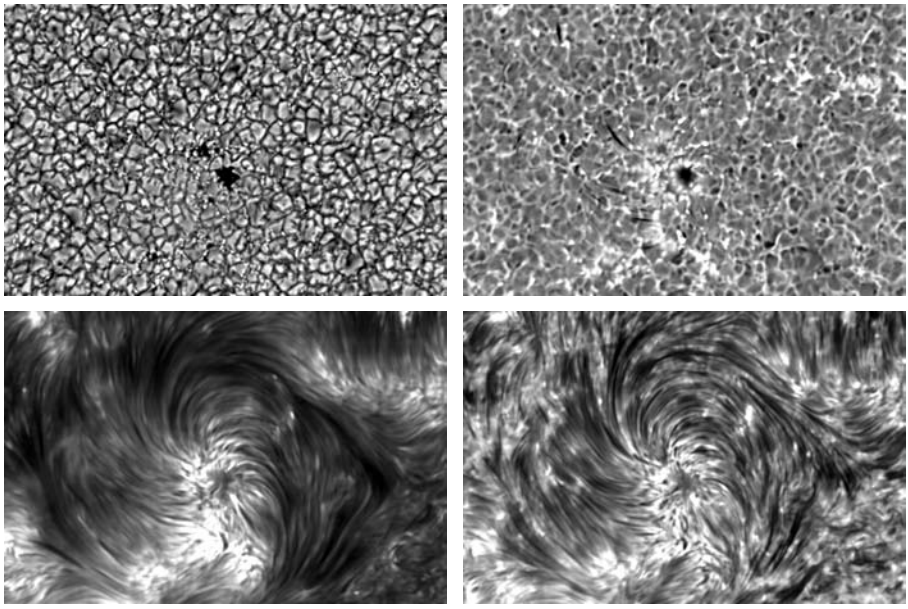

Figure 11. Near-simultaneous images taken with IBIS at the DST on October 1, 2005 using adaptive optics and speckle reconstruction, clockwise in white light and in Ca II 8542 Å at $\Delta\lambda = -600$, -200, and 0 mÅ from line center. Field about 60×40 arcsec^2. Courtesy G. Cauzzi.

from Dopplershifts (cf. Cauzzi et al. on p. 127 ff). The outer-wing panel shows the upper-photospheric mesh of reversed granulation with acoustic brightenings (cf. Rutten 2003b) very markedly, suggesting that the temperature sensitivity does not cause as wide a formation gap as the Hα jump from normal (or flattened, see Leenaarts & Wedemeyer-Böhm 2006) granulation to chromospheric fibrils.

Combining Hα and Ca II 8542 with full profile sampling may permit disentangling Dopplershift, thermal line broadening, and source function variation since their atomic mass difference produces large difference in thermal Dopplerwidth. Dopplerwidth measurement may provide a more direct handle on fibrilar temperature than fibril brightness, most awkwardly set by NLTE opacity and source function complexities for Hα.

3.3. Ly-α chromosphere

Figure 12 shows a beautiful Ly-α image. Towards the limb it is remarkably similar to the outer-wing Hα scene (Fig. 7) but with reversed contrast: bright hedge rows of short upright fibrils jut out at network borders of cells; the latter are covered by flatter and darker extended-fibril canopies. The rows of stubby fibrils appear similar to oscillation-loaded dynamic fibrils in Hα. They seem optically thick so that their brightness implies enhanced source function, either through $S = (1-\varepsilon)J + \varepsilon B$ resonance-scattering with small ε or through Balmer and higher recombination adding an ηB^* term. Both mechanisms suggest high

Figure 12. Ly-α image from the second flight of the VAULT rocket telescope (Korendyke et al. 2001; Vourlidas et al. 2001; `http://wwwsolar.nrl.navy.mil/rockets/vault`). Field 246×384 arcsec^2. The passband contains the full line. Courtesy A. Vourlidas.

temperature. The probable identity of Hα and Ly-α fibrils implies that the latter are thin hot sheaths around the former.

The extended active-region plage towards the bottom of the image appears very grainy, suggestive of mossy plage in TRACE 171 Å movies (e.g., Berger et al. 1999; Fletcher & de Pontieu 1999; de Pontieu et al. 1999).

3.4. Hα and Fe 171 chromosphere

Finally, Fig. 13 compares the appearance of an active region in Hα images from the DOT and in Fe 171 Å images from TRACE (movie: `http://dot.astro.uu.nl/movies`). The G-band image illustrates that granulation remains visible even in one-hour averaging. The Ca II H wing image represents an unsigned magnetogram because reversed granulation vanishes better through temporal averaging. This was done here to emphasize the overall bright-dark patterns in the remaining images. They are strikingly similar between Hα line-center brightness and Fe 171 brightness. The first should sample 10^4 K gas, the latter 10^6 K gas; the close similarity therefore needs consideration.

Hα is bright either due to large chromospheric emissivity or due to sufficiently small chromospheric opacity that one sees into the underlying deep photosphere. Note that the latter is certainly the case in umbrae since they display umbral dots even at Hα line center (also in this figure), implying absence of chromospheric opacity. Bright-dark contrast between otherwise similar fibrils may come from larger thickness of the darker ones, having lower scattering source functions at their surface. Excess emissivity may result from excess excitation and from excess recombination. The latter may arise in steep-gradient neutral-to-coronal interfaces or through the Zanstra mechanism as for planetary-nebulae Balmer emission.

Fe 171 is bright solely through thermal photon creation but is dark in two ways: either through absence of emissivity along the line of sight into the black photospheric or sky background[2], or through blocking of thermal background brightness by foreground bound-free out-of-the-passband scattering in the H I, He I and/or He II continua as explained in Fig. 10 of Rutten (1999a).

The bright blob at image center appears similarly in Fe 171, at Hα line center, and in the Hα wing summation. The Fe 171 blob suggests a relatively dense cloud of 10^6 K gas. The Hα brightness either results from chromospheric transparency or from chromospheric emissivity. Whichever of the two, it must correlate with the presence of very hot gas. Hydrogen ionization may explain excess transparency, recombination excess emissivity.

4. Speculations

My impressions from the images in the previous section are:

- the chromosphere consists of the mass (or mess) of fibrils observed in Hα;
- cell-spanning fibrils outline magnetic canopies. Above quiet cell centers they are jostled and kicked up by upward-propagating shocks, producing an extended cool clapotisphere underneath;

[2]The term "volume blocking" is nonsensical since a volume doesn't block by itself. It is used to express lack of emissivity along a line of sight through some volume, an "emissivity void" – but a void doesn't block either; lack of emissivity cannot be expressed as opaqueness.

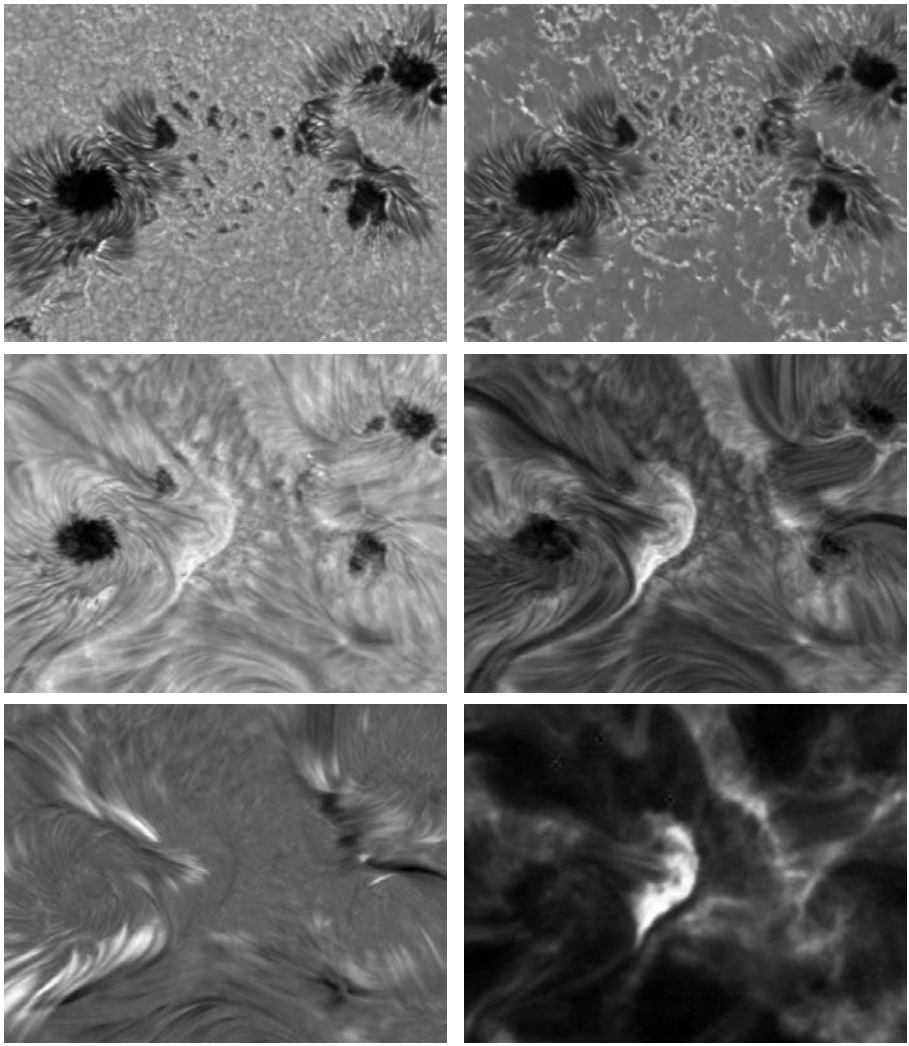

Figure 13. One-hour temporal averages of co-aligned DOT and TRACE image sequences taken on July 9, 2005. *Top*: G band; Ca II H at $\Delta\lambda = -2.35$ Å from line center. *Middle*: sum of Hα at $\Delta\lambda = \pm 500$ mÅ; Hα line center. *Bottom*: difference of Hα at $\Delta\lambda = \pm 500$ mÅ (Dopplershift, upward dark); TRACE 171 Å. Field size 78×60 arcsec^2. The bright blob in Hα and Fe 171 is sharply delineated at right, presumably at the neutral line through this active region. The Hα wing difference indicates marked absence of large Dopplershifts in this area, without fibrilar structuring (best seen by zooming in with a pdf viewer). Courtesy A. G. de Wijn.

– slanted fields jutting out from network and plage suffer oscillatory cool-gas loading to become dynamic fibrils (De Pontieu et al. 2007) and EUV shutters

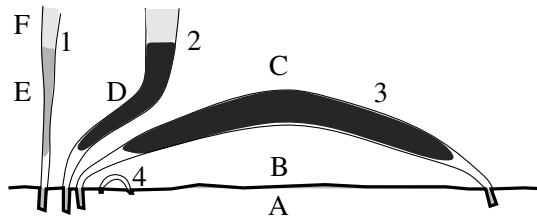

Figure 14. Different types of fibrils together constituting the chromosphere. Rough temperatures: D$\sim 10^4$ K, E$\sim 10^5$ K, F$\sim 10^6$ K. Outside regimes: A = photosphere with normal/reversed granulation and relatively empty magnetic elements, B = subcanopy "clapotisphere" pervaded by acoustic shocks but otherwise cool, C = coronally transparent in H&K, Hα, and Ly-α. Type 1: bright upright network straws opening into coronal plasma. Type 2: dark Hα fibrils bending upward into hot plasma from unipolar crowding. Type 3: dark Hα fibrils spanning across cell interiors in bipolar network outling magnetic canopies. Type 4: short weak-field near-network loops postulated by Schrijver & Title (2003). From Rutten (2007).

(De Wijn et al. 2007). These possess transition-interface sheaths that are optically thick in Ly-α;

- more straight-up fields above network and plage show up as bright Ca II straws and bright Hα fibril feet, likely through recombination emissivity. Near the limb they appear as hedge rows that are bright in Ca II and Ly-α but dark in the outer Hα wings from bright background, large Dopplershift, and/or large thermal broadening.
- near-vertical fields in active regions produce graininess in Ly-α, mossy plage, and brightness correspondence between Hα and Fe 171. They provide locations where hot gas comes very close to the photosphere, presumably through downward conduction and lack of upward kicking.

These impressions are cartoonized in Fig. 14, copied from Rutten (2007) where I summarized them without showing so many tell-tale images.

5. Suggestions

We obviously need improved Hα imaging. Combination with Hβ and one or more of the Ca II IR lines is desirable. Yet better is multi-line chromospheric imaging with synchronous co-spatial Dopplergrams and magnetograms of the underlying photosphere and with TRACE/SDO EUV imaging of the higher-temperature scenes. All this in long-duration movie sequences. Unfortunately, Hinode's tunable filter seems not fulfilling its intended Hα capability (but would anyhow deliver only slow cadence due to telemetry limitations).

The Hα images in Figs. 6–10 illustrate the necessity of high angular resolution. Because Hα fibrils appear as high-lying Schuster-Schwarzschild clouds which may be optically thin, there is no smallest-scale limit set by mean-free photon paths or scattering lengths. In addition, their dynamical behavior necessitates taking sustained-quality image sequences at fast cadence. The DOT does so admirably, but the twice larger SST yields not only higher resolution

but also better signal-to-noise through better cameras, better alignment through MOMFBD restoration (Van Noort et al. 2005), and especially faster cadence because MOMFBD requires fewer frames than speckle reconstruction. Van Noort & Rouppe van der Voort (2006) demonstrated that imaging cadence as fast as 1 fps is needed for some Hα dynamics, well beyond the traditional estimate of soundspeed travel across a resolution element.

In addition, one should add line-profile sampling to disentangle the complex cross-talk between opacity, source function, and Dopplershift variations. Chromospheric imaging at high resolution so becomes just as photon-starved as photospheric spectropolarimetry at high resolution, making fast-cadence profile-sampling narrow-band imaging a second motivation for telescope aperture beyond the angular resolution in reach of AO and post-detection processing. Post-focus light handling is presently done best by rapid-scan Fabry-Pérot imaging. Fiber field reformatting may enable 2D MOMFBD spectrometry in the future (Rutten 1999b).

The obvious desire to add ultraviolet spectrometry at high angular resolution to sample hot fibril sheaths is presently unanswered: no HRTS- or SUMER-like spectrometer is available for regular co-pointing. Even better would be integral-field ultraviolet profile sampling because slits, whether scanning or sitting-and-staring, tend to be at the wrong place at the wrong time. The lack of such ultraviolet instrumentation is the major longer-term deficiency in chromospheric observing, making Hα the key diagnostic by default.

The simple question "where is this line formed?" discussed in Section 2 is a naïve way of asking "how well does my interpretation fit reality?", a question well beyond observation. So let me end by addressing modeling options.

The SIR technique thanks its large success in its main application, photospheric Stokes profile inversion, to the same reasons why Holweger's line fitting made HOLMUL such a success in abundance determination: LTE and smooth radial behavior are good assumptions for photospheric iron lines. Extension to scattering and sinusoidal waves around $h = 500$ km is doable (outside sunspots) within such inversion approaches, but already the shocked clapotisphere below the canopy needs forward modeling based on numerical simulations.

The fibrilar chromosphere surely requires simulation physics to diagnose its structural and dynamical physics; the breakthrough example is Hansteen's simulation in De Pontieu et al. (2007). The chromosphere cannot be treated by inversion before its physics is understood, and then only if all fibrils are so similar in geometry, temperature, density, etc., that multi-cloud modeling (with some sort of NLTE radiative transfer in and between each) remains realistically limited in parameter space. The interpretational path to follow is forward modeling based on 2D and 3D simulations. However, PANDORA-style 1D modeling suits to study radiative transfer in and between fibrils with transition sheaths in full detail for working out and testing simpler recipes for multi-D codes. This step is similar to studying transition-sheath radiation in and from prominences as by Schwartz et al. (2006).

Shortcutting through untested tractability assumptions is dangerous even though it may produce intrinsically interesting "code-as-a-star" papers.

Acknowledgments. I thank the CSPM organizers for a very good meeting and for inviting me to both speakership and editorship. My participation was funded by the Leids Kerkhoven-Bosscha Fonds and the EC-RTN European Solar Magnetism Network.

References

Athay R. G., 1976, in C. J. Cannon (ed.), Interpretation of Atmospheric Structure in the Presence of Inhomogeneities, Comm. 12, General Assembly IAU, Grenoble, Univ. Sydney, Sydney, 69
Avrett E. H., 1985, in B. W. Lites (ed.), Chromospheric Diagnostics and Modeling, NSO/SP Summer Conference, Sunspot, 67
Beckers J. M., Milkey R. W., 1975, Solar Phys. 43, 289
Berger T. E., de Pontieu B., Schrijver C. J., Title A. M., 1999, ApJ 519, L97
Bloomfield D. S., McAteer R. T. J., Mathioudakis M., Williams D. R., Keenan F. P., 2004, ApJ 604, 936
Bruls J. H. M. J., Rutten R. J., Shchukina N. G., 1992, A&A 265, 237
Cabrera Solana D., Bellot Rubio L. R., del Toro Iniesta J. C., 2005, A&A 439, 687
Caccin B., Gomez M. T., Marmolino C., Severino G., 1977, A&A 54, 227
Carlsson M. (ed.), 1994, Chromospheric Dynamics, Proc. Mini-workshop, Inst. Theor. Astrophys., Oslo
Carlsson M., Rutten R. J., Shchukina N. G., 1992, A&A 253, 567
Carlsson M., Stein R. F., 1992, 397, L59
Carlsson M., Stein R. F., 1997, ApJ 481, 500
Carlsson M., Stein R. F., 2002, ApJ 572, 626
de Pontieu B., Berger T. E., Schrijver C. J., Title A. M., 1999, Solar Phys. 190, 419
De Pontieu B., Hansteen V. H., Rouppe van der Voort L., van Noort M., Carlsson M., 2007, ApJ 655, 624
De Wijn A. G., De Pontieu B., Rutten R. J., 2007, ApJ 654, 1128
De Wijn A. G., Rutten R. J., Tarbell T. D., 2005, A&A 430, 1119
del Toro Iniesta J. C., 2003, Astronomische Nachrichten 324, 383
Dowd J., 1981, Sea Kayaking, Univ. Washington Press, Seattle
Edmonds, Jr. F. N., 1967, AJ 72, 793
Fletcher L., de Pontieu B., 1999, ApJ 520, L135
Fontenla J. M., Avrett E., Thuillier G., Harder J., 2006, ApJ 639, 441
Fontenla J. M., Avrett E. H., Loeser R., 1993, ApJ 406, 319
Fossum A., Carlsson M., 2005a, Nat 435, 919
Fossum A., Carlsson M., 2005b, ApJ 625, 556
Fossum A., Carlsson M., 2006, ApJ 646, 579
Gurtovenko E. A., Ratnikova V. A., 1974, AZh 51, 1032
Holweger H., 1967, Z. f. Astrophysik 65, 365
Holweger H., Müller E. A., 1974, Solar Phys. 39, 19
Jefferies S. M., McIntosh S. W., Armstrong J. D., Bogdan T. J., Cacciani A., Fleck B., 2006, ApJ 648, L151
Judge P. G., 2007, in H. Uitenbroek, J. Leibacher, R. F. Stein (eds.), Solar MHD: Theory and Observations, Procs. 23rd NSO workshop, ASP Conf. Ser. 354, 265
Keller C. U., Schüssler M., Vögler A., Zakharov V., 2004, ApJ 607, L59
Korendyke C. M., Vourlidas A., Cook J. W., Dere K. P., Howard R. A., Morrill J. S., Moses J. D., Moulton N. E., Socker D. G., 2001, Solar Phys. 200, 63
Krijger J. M., Rutten R. J., Lites B. W., Straus T., Shine R. A., Tarbell T. D., 2001, A&A 379, 1052
Kucera A., Balthasar H., Rybak J., Wöhl H., 1998, A&A 332, 1069
Leenaarts J., Rutten R. J., Sütterlin P., Carlsson M., Uitenbroek H., 2006, A&A 449, 1209
Leenaarts J., Wedemeyer-Böhm S., 2006, A&A 460, 301

Lites B. W. (ed.), 1985, Chromospheric Diagnostics and Modeling, Proceedings NSO Summer Conference, Sunspot
Magain P., 1986, A&A 163, 135
Maltby P., Avrett E. H., Carlsson M., Kjeldseth-Moe O., Kurucz R. L., Loeser R., 1986, ApJ 306, 284
Mein P., 1971, Solar Phys. 20, 3
Neckel H., 1999, 184, 421
Pecker J.-C., 1951, Annales d'Astrophysique 14, 115
Ruiz Cobo B., del Toro Iniesta J. C., 1992, ApJ 398, 375
Ruiz Cobo B., del Toro Iniesta J. C., Collados M., Sánchez Almeida J., 1990, Ap&SS 170, 113
Rutten R. J., 1990, in G. Wallerstein (ed.), Cool Stars, Stellar Systems and the Sun, Proc. Sixth Cambridge Workshop, ASP Conf. Ser. 9, 91
Rutten R. J., 1995, in J. T. Hoeksema, V. Domingo, B. Fleck, B. Battrick (eds.), Helioseismology, Proc. Fourth SOHO Workshop, ESA SP–376 Vol. 1, ESA Publ. Div., ESTEC, Noordwijk, 151
Rutten R. J., 1998, in C. Fröhlich, M. C. E. Huber, S. Solanki, R. von Steiger (eds.), Solar Composition and its Evolution – from Core to Corona, Procs. ISSI Workshop, Space Sci. Rev. 85, 269
Rutten R. J., 1999a, in B. Schmieder, A. Hofmann, J. Staude (eds.), Magnetic Fields and Oscillations, Procs. Third Adv. in Solar Physics Euroconf., ASP Conf. Ser. 184, 181
Rutten R. J., 1999b, in T. R. Rimmele, K. S. Balasubramaniam, R. R. Radick (eds.), High Resolution Solar Physics: Theory, Observations, and Techniques, Procs. 19th NSO/Sacramento Peak Summer Workshop, ASP Conf. Ser. 183, 296
Rutten R. J., 2002, Jour. Astron. Data 8, 8
Rutten R. J., 2003a, Radiative Transfer in Stellar Atmospheres, Lecture Notes Utrecht University, 8th Edition, `http://www.astro.uu.nl/~rutten`
Rutten R. J., 2003b, in R. von Fay-Siebenbürgen, K. Petrovay, J.-L. Ballester, M. Aschwanden (eds.), Turbulence, Waves and Instabilities in the Solar Plasma, NATO ASI Series II 124, Kluwer, Dordrecht, 137
Rutten R. J., 2007, in H. Uitenbroek, J. Leibacher, R. F. Stein (eds.), Solar MHD: Theory and Observations, Procs. 23rd NSO workshop, ASP Conf. Ser. 354, 282
Rutten R. J., Kostik R. I., 1982, A&A 115, 104
Rutten R. J., Uitenbroek H., 1991a, Solar Phys. 134, 15
Rutten R. J., Uitenbroek H., 1991b, in P. Ulmschneider, E. R. Priest, R. Rosner (eds.), Mechanisms of Chromospheric and Coronal Heating, Proc. Heidelberg Conf., Springer, Berlin, 48
Schoolman S. A., 1972, Solar Phys. 22, 344
Schrijver C. J., Title A. M., 2003, ApJ 597, L165
Schwartz P., Heinzel P., Schmieder B., Anzer U., 2006, A&A 459, 651
Skartlien R., Stein R. F., Nordlund Å., 2000, ApJ 541, 468
Socas-Navarro H., Trujillo Bueno J., Ruiz Cobo B., 2001, ApJ 550, 1102
Uitenbroek H., Bruls J. H. M. J., 1992, A&A 265, 268
Unsöld A., 1955, Physik der Sternatmosphären, Springer, Berlin
van Noort M., Rouppe van der Voort L., Löfdahl M. G., 2005, Solar Phys. 228, 191
van Noort M. J., Rouppe van der Voort L. H. M., 2006, ApJ 648, L67
Vernazza J. E., Avrett E. H., Loeser R., 1981, ApJS 45, 635
Vourlidas A., Klimchuk J. A., Korendyke C. M., Tarbell T. D., Handy B. N., 2001, ApJ 563, 374
Wedemeyer-Böhm S., Steiner O., Bruls J., Rammacher W., 2007, in P. Heinzel, I. Dorotovič, R. J. Rutten (eds.), The Physics of Chromospheric Plasmas, Coimbra Solar Physics Meeting, ASP Conf. Ser. 368, 93
Zirin H., 1988, Astrophysics of the Sun, Cambridge Univ. Press, Cambridge UK